



CrossMark
click for updates

Cite this: *RSC Adv.*, 2016, 6, 15861

Morphology-controlled synthesis of highly crystalline Fe_3O_4 and CoFe_2O_4 nanoparticles using a facile thermal decomposition method

Yunji Eom,^{†a} Mohamed Abbas,^{†ab} HeeYoon Noh^a and CheolGi Kim^{*a}

CoFe_2O_4 and Fe_3O_4 nanoparticles with controllable morphology were synthesized using a convenient and facile one-pot thermal decomposition method. Iron(III) acetylacetonate and cobalt(II) acetylacetonate were used as precursors instead of the toxic and expensive pentacarbonyl, and oleic acid and oleylamine employed as solvents, stabilizers, and reducing agents. The nanoparticles exhibit well-defined shapes of varying size and their morphology can be tuned by modifying the reaction time, solvent, and temperature. Transmission electron microscopy, energy dispersive spectroscopy and X-ray diffraction were utilized to confirm the unique morphology, high crystallinity, composition and pure phase structure. Magnetic characterization of the nanoparticles further revealed the highest saturation magnetization value of 80.93 and 92.94 emu per g obtained for the cubic shape in the case of both CoFe_2O_4 and Fe_3O_4 , respectively.

Received 24th December 2015
Accepted 26th January 2016

DOI: 10.1039/c5ra27649g

www.rsc.org/advances

1. Introduction

Magnetic nanoparticles (MNPs) have been studied extensively within the last decade and till now in part due to their diverse potential for application in biomedicine, catalysis, electronic and energy fields.^{1–3} Ferrite nanoparticles (NPs) in particular have been comprehensively investigated for a variety of applications due to their unique magnetic properties, high electrical resistivity, mechanical properties, and high chemical stability.^{4,5} However, the potential application of MNPs in a number of fields will depend on the ability to produce materials with high crystallinity, stability, dispersion, and magnetic behavior. Notably, NPs have a tremendous impact on the resulting properties and potential applications. Indeed, changing the crystal shape of nanoparticles alters the exposed crystal facets and hence atomic arrangements in each facet which will have significant effect on its various properties.⁶

Various approaches including sonochemical, polyol, and hydrothermal synthesis, microemulsion, thermal decomposition, and co-precipitation^{5,7–11} have been used to target ferrite NPs with various sizes and morphologies. Among these methods, thermal decomposition is considered the most attractive approach for accessing ferrite NPs with high crystallinity and uniform particle size distribution.¹

In our previous work, we used the sonochemical technique to synthesize Fe_3O_4 and CoFe_2O_4 nanoparticles with high

crystallinity and large magnetic moment,^{5,12} however, the extent of control over particle dispersion and morphology was not adequate for achieving particles useful in real applications. In this paper, we present a facile, safe, and convenient thermal decomposition route for morphology controlled synthesis of two kinds of ferrite of Fe_3O_4 and CoFe_2O_4 . Moreover, in our synthesis approach, we avoid the using of complex procedures in terms of the needed to prepare an intermediate product such as iron oleate and or using excess amount of surfactants (*e.g.*, 1,2-hexadecanediol, and octadecanol, 1-octadecene, *etc.*) which used in previous reports of thermal decomposition method.^{13–16} Thus, simple modification of the reaction condition allowed us to isolate nanoparticles as cubes, hexagons and spheres with sizes ranging from 6 to 96 nm. Oleic acid and oleylamine were used as the solvents, stabilizers, and reducing agents¹⁷ and iron(III) acetylacetonate and cobalt(II) acetylacetonate were successfully employed as precursors instead of commonly used toxic, flammable and expensive pentacarbonyl.^{18,19} The Fe_3O_4 and CoFe_2O_4 nanoparticle morphology, composition and crystalline structure were monitored using X-ray diffraction (XRD), transmission electron microscope (TEM), high resolution transmission electron microscopy (HRTEM), energy dispersive spectroscopy (EDS) and their magnetic properties were characterized using superconducting quantum interference device (SQUID) from -15 kOe to $+15$ kOe at 300 K.

2. Experimental section

2.1 Materials

Iron(III) acetylacetonate (97%), cobalt(II) acetylacetonate (98%), benzyl ether (98%), oleic acid (99%), oleylamine (98%) were

^aDepartment of Emerging Materials Science, DGIST, 711-873 Daegu, South Korea. E-mail: cgkim@dgist.ac.kr; Fax: +82-53-785-6509; Tel: +82-53-785-6516

^bCeramics Department, National Research Centre, 12622 El-Bohouth Str., Cairo, Egypt

[†] The first and second authors are contributed equally to this paper.

purchased from Sigma-Aldrich, Ltd. All of the chemicals were of analytical reagent grade and used as received without any further purification.

2.2 Synthesis of CoFe₂O₄ nanoparticles

Three shapes of sphere, cube, and hexagonal of CoFe₂O₄ NPs were synthesized using thermal decomposition method. Firstly, for synthesis of CoFe₂O₄ nanosphere, suitable amount of iron(III) acetylacetonate and cobalt(II) acetylacetonate were dispersed in 40 mL benzyl ether as solvent media in three neck round-bottom flask using mechanical stirrer. After that, 3 mL of each oleic acid and oleylamine were added simultaneously to the above solution. The mixture was heated to 100 °C with a heating rate of 10 °C min⁻¹ and kept for 60 min at this temperature. Thereafter, the reaction temperature was increased to 290 °C with a heating rate of 10 °C min⁻¹ and kept refluxing for 45 min. The mixture was cooled down to room temperature naturally and then collected the precipitate using a permanent magnet. The collected CoFe₂O₄ nanoparticles were washed using a mixture solvent of acetone and ethanol at room temperature to remove any impurities. The washing process repeated for five times and in every time the magnetic nanoparticles were collected using a permanent magnet.

For the synthesis of CoFe₂O₄ nanocubes, we used the same procedures mentioned above with decreasing the amount of benzyl ether to 20 mL and using only oleic acid (2.5 mL) as reducing agent with reducing the reaction time to be 30 min at 290 °C. For synthesis of hexagonal shape of CoFe₂O₄ NPs, we further decreasing the amount of benzyl ether to 15 mL and increasing the reaction time to 90 min at 290 °C.

2.3 Synthesis of Fe₃O₄ nanoparticles

Fe₃O₄ nanoparticles with two different shapes of nanocubes and nanohexagonal were also synthesized using the same procedures used in case of CoFe₂O₄ NPs of thermal decomposition method. For a typical synthesis of Fe₃O₄ nanocubes, 3 mmol of iron(III) acetylacetonate was mixed with 15 mL benzyl ether and 3 mL oleic acid using mechanical stirring in three neck round-bottom flask. The mixture was heated to 100 °C with a heating rate of 10 °C min⁻¹ and kept at this temperature for 60 min, and then the temperature increased to 260 °C with refluxing for 90 min. The mixture was cooled down to room temperature naturally and then we collected the precipitate using a permanent magnet. The collected Fe₃O₄ nanocubes were washed using a mixture solvent of acetone and ethanol at room temperature to remove any impurities. The washing process repeated for five times and in every time the magnetic nanoparticles were collected using a permanent magnet. For synthesis of Fe₃O₄ nanohexagonal, we used the same procedures mentioned above exactly with increasing only the temperature up to 290 °C.

2.4 Characterization

The crystal structures of the as-synthesized CoFe₂O₄ and Fe₃O₄ nanoparticles were analyzed using X-ray powder diffraction (XRD, Rigaku D/max-250) with Cu K α radiation ($\lambda = 1.540562 \text{ \AA}$)

in the 2θ range from 20 to 80°. The morphology and size of the nanoparticles were characterized using transmission electron microscopy (TEM, the Tecnai G2 F20 operated at 300 kV) and high resolution transmission electron microscopy (HRTEM). And the chemical compositions of the nanoparticles were analyzed by an EDS analysis which coupled with the TEM equipment. The magnetic properties of the nanoparticles were measured by superconducting quantum interference device (SQUID) from -15 kOe to +15 kOe at room temperature.

3. Results and discussion

A facile thermal decomposition route was designed in our study for producing different shapes and sizes of Fe₃O₄ and CoFe₂O₄ nanoparticles. Noteworthy, in the most of recently reported works for synthesis of ferrite NPs using thermal decomposition method, they used much amount of surfactant and reducing agent, like 1,2-hexadecanediol and octadecanol, *N*-nitrosophenylhydroxylamine, *etc.*,¹³ and or complicated procedure including the synthesis of iron oleate complex as intermediate then thermal decomposition.¹⁴ Indeed, several studies have reported that controlling the nucleation and growth dynamics by modifying the heating rate, temperature, and the precursor concentration can result in the formation of various shaped nanocrystals.²⁰ However, in this study, the morphology controlled of the nanoparticles was successfully achieved through the modification of reaction parameters, includes reaction temperature and the amount of benzyl ether as a solvent.

The morphology of the as-synthesized CoFe₂O₄ and Fe₃O₄ nanoparticles was investigated using transmission electron

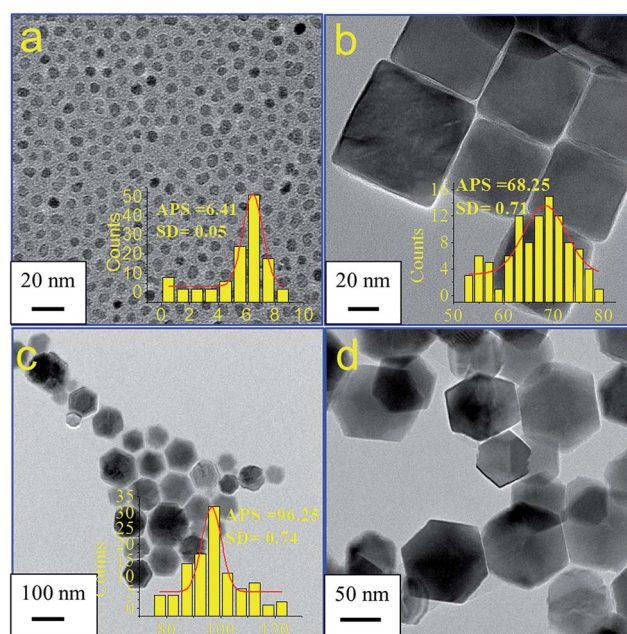


Fig. 1 TEM images of CoFe₂O₄ nanoparticles with different shapes (a) sphere shape, (b) cube shape and (c and d) hexagonal shape. The inset is a statistical analysis of the nanoparticles including average particles size (APS) and the standard deviations (SD).

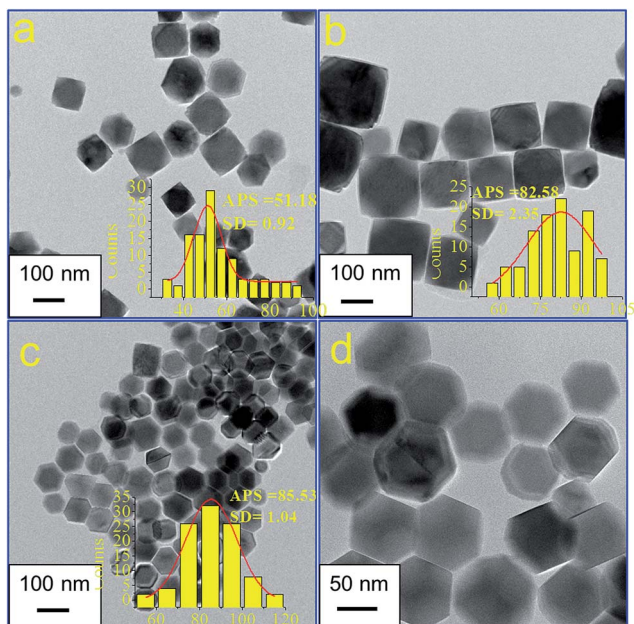


Fig. 2 TEM images of Fe_3O_4 nanoparticles with different shapes (a and b) cube shape and (c and d) hexagonal shape. The inset is a statistical analysis of the nanoparticles including average particles size (APS) and the standard deviations (SD).

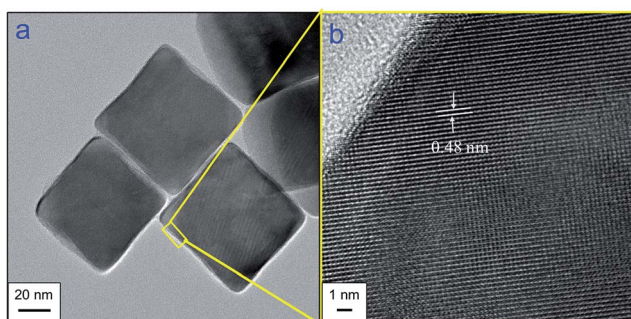


Fig. 3 TEM and HRTEM images of Fe_3O_4 nanocubes.

microscopy. A statistical analysis has been done for each sample of CoFe_2O_4 and Fe_3O_4 nanoparticles through counting 100 particles, and the average particles size (APS) as well as standard deviations (SD) are estimated from TEM micrograph using the lognormal distribution (see inset of Fig. 1 and 2). Fig. 1 shows different TEM images of CoFe_2O_4 nanoparticles with various shapes. Monodisperse sphere-like shapes of 6.41 nm size of CoFe_2O_4 nanoparticle were obtained when we used 40 mL of benzyl ether and 3 mL of each oleic acid and oleylamine for 45 min of refluxing time (Fig. 1a). However, highly crystalline nanocube with average particles size of 68.25 nm were produced when the amount of solvent was decreased to 20 mL while using oleic acid as a sole reducing agent at 30 min refluxing time (Fig. 1b). Interestingly, further decreasing of the solvent amount to 15 mL and increasing the reaction time to 90 min resulted in evolution of the nanocubes shape to be hexagonal with medium particle size of 96.65 nm (Fig. 1c and d). The shape evolution of the nanoparticles in our study is mainly ascribed to the crucial role of the surfactant and reaction time. Hence, increasing the ratio of surfactant to solvent and also prolonging the reaction time at 260 °C to 90 min, not only does the {111} surface show saturated surface coverage, the surface {100} is also coordinated by the capping ligand, resulting in hexagon shapes with both {100} and {111} surfaces well developed.²¹

Fig. 2 shows the TEM images of the as-synthesized Fe_3O_4 nanoparticles with two different shapes of cubic and hexagonal. Fig. 2a shows TEM images of Fe_3O_4 nanocubes with average particles size distribution of 51.18 nm obtained at 260 °C refluxing temperature and 90 min of reaction time. On the same time, when we prolonged the time of reaction to 120 min, the size of the nanocubes increased to be 82.58 nm (Fig. 2b). However, increasing the reaction temperature to 290 °C, produced a hexagonal shapes of Fe_3O_4 NPs as appears clearly in Fig. 2c and d and the average particles size increased to be 85.53 nm. The formation of the hexagonal shapes here may be attributed to the continuous growth at 290 °C along the corners of the cubic shape. For more detail of magnetite NPs structure, we used HRTEM to observe the single-crystallinity of the Fe_3O_4 nanocubes as appear in Fig. 3. The interplanar distance

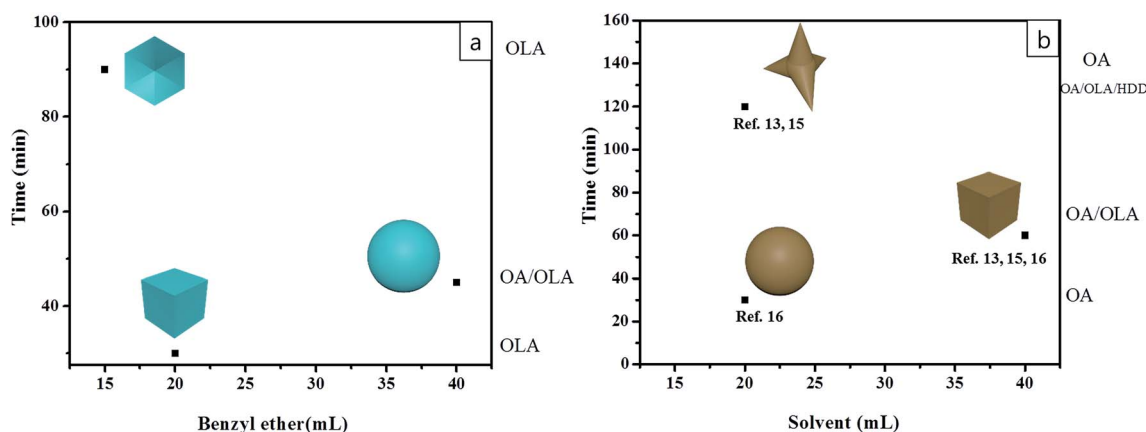


Fig. 4 Schematic diagram of morphological evolution of CoFe_2O_4 NPs under different synthetic conditions (a) in case of this study and (b) in case of other reported works (ref. 13, 15, and 16).

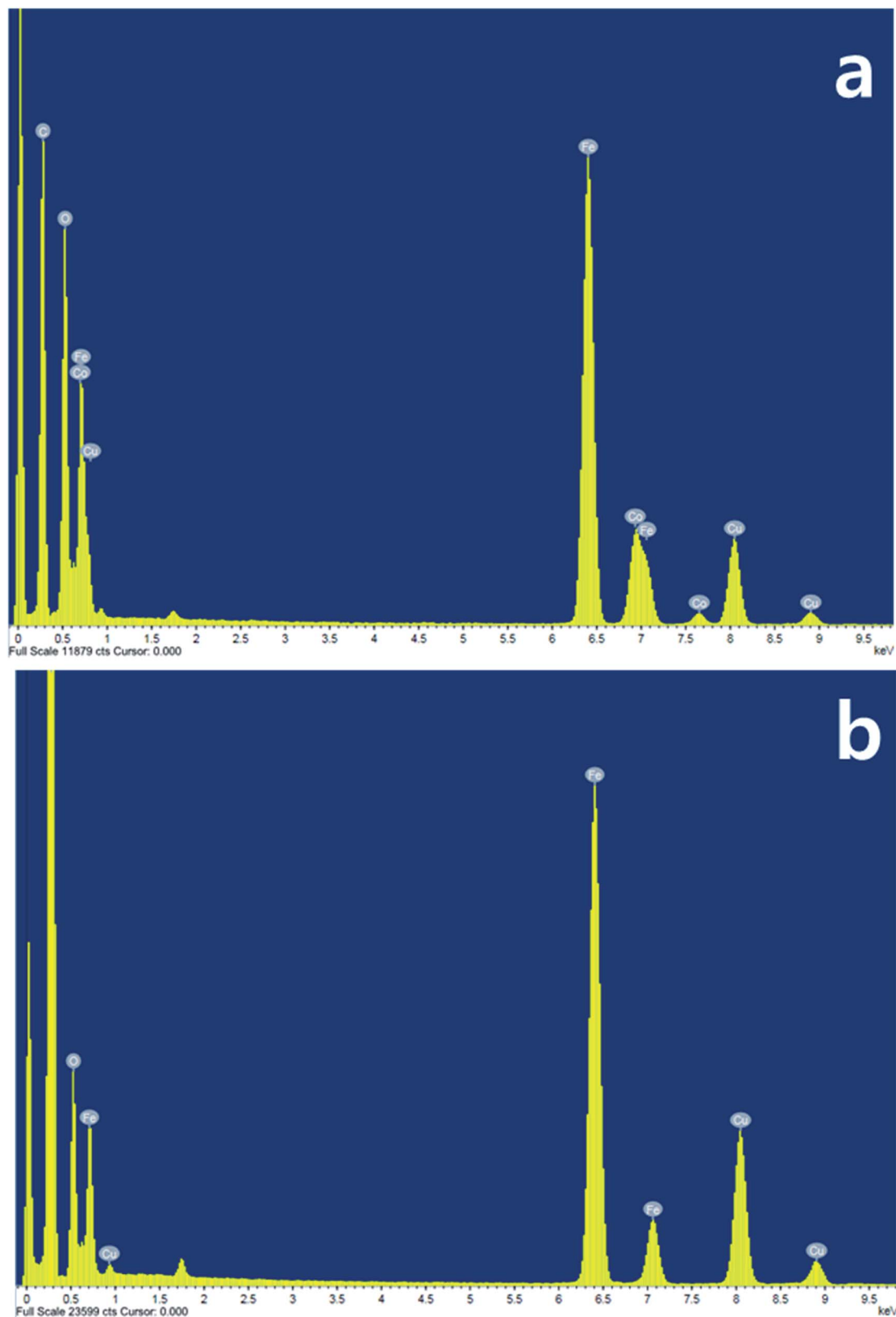


Fig. 5 EDS elemental analysis of (a) CoFe₂O₄ NPs and (b) Fe₃O₄ NPs.

measured from the adjacent lattice fringes in Fig. 3b is about 0.48 nm, which corresponding to (111) planes of the Fe₃O₄ single crystal with cubic inverse spinel structure.^{22,23} For easy

understand of the relation between the reaction parameters and morphology controlling, Fig. 4 shows a schematic diagram for the morphological evolution of CoFe₂O₄ NPs under different

synthetic conditions. Fig. 4a represents the schematic of the obtained nanoparticles in our study within the three different shapes of sphere, cubes and hexagons. And, Fig. 4b concluded the other recently reported works for the synthesis of the various shapes of CoFe_2O_4 NPs. Lu *et al.* and Zhang *et al.* reported the synthesis of two different shapes of cubes and star-like CoFe_2O_4 NPs,^{13,15} however, Baaziz *et al.* synthesized two shapes of cubes and sphere CoFe_2O_4 NPs using thermal decomposition method.¹⁶

Fig. 5 shows the EDS spectrum analysis for both samples of CoFe_2O_4 and Fe_3O_4 NPs. From the figure, there are mainly three elements of iron, oxygen and cobalt were observed for the CoFe_2O_4 NPs sample (Fig. 5a), however, only iron and oxygen were detected for the second sample of Fe_3O_4 NPs (Fig. 5b), confirmed the elemental composition of both samples. Since, because we employed the carbon copper grid in the measurements, there are two additional peaks in the spectrum for Cu and C were detected.

The crystal structure, phases and purity of the as-synthesized CoFe_2O_4 and Fe_3O_4 nanoparticles were investigated through the X-ray diffraction (XRD) with Cu $K\alpha$ radiation ($\lambda = 1.540562 \text{ \AA}$). Fig. 6 shows the XRD diffraction patterns of the three different shapes of sphere, cube and hexagonal CoFe_2O_4 nanoparticles. From the figure, it is found that all of the diffraction peaks in the three patterns of the crystal planes (220), (311), (222), (400), (422), (511), and (533) could be indexed to a cubic inverse spinel structure of CoFe_2O_4 NPs, which are consistent with the standard data for the ferrite phase (JCPDS card no. 00-019-0629).⁵ Additionally, no other impurity phases were detected in the patterns, reflecting the high purity phase of the as-synthesized CoFe_2O_4 nanoparticles under current mild experimental condition. Further, the crystallite particle size of the three shapes of CoFe_2O_4 nanoparticles were calculated from the XRD pattern using Debye-Scherrer formula of ($D = K\lambda/\beta \cos \theta$), where λ is the X-ray wavelength (1.540562 \AA), β is the full width at half maximum (FWHM), θ is the Bragg angle for the studied peak per ring, and K is the shape factor which is normally taken

as 0.9 for ferrites.^{23,24} Based on the calculation, we found an agreement between the calculated crystallite particle size from XRD data (7.5 nm) and the estimated particles size from the TEM images (6.41 nm) for the sphere shape of CoFe_2O_4 NPs, and it's may be attributed to the good dispersion of the sample as appeared from the TEM images. However, a disagreement between the calculated crystallite particle size from XRD data (19.5 and 23.5 nm) and the estimated particles size from the TEM images (68.25 and 96.65 nm) was found for the cubic and hexagonal shapes, respectively of CoFe_2O_4 NPs, and this difference may be attributed to the polydispersity nature of the nanoparticles as displayed from the TEM images.

On the other hand, the as-synthesized Fe_3O_4 nanoparticles with their two shapes of cubic and hexagonal displayed the same crystal planes and indexed to a cubic inverse spinel structure of Fe_3O_4 within sharp and high intensity peaks (Fig. 7). Further, even though it's too difficult to distinguish between the two phases of magnetite (Fe_3O_4) and maghemite ($\gamma\text{-Fe}_2\text{O}_3$) through the XRD peaks, but the obtained completely black color in our samples, may be suggest that the magnetite is the dominant phase.²⁵ The lattice parameters were calculated using the following eqn (1) and (2).^{26,27} Using these equations, we calculated the lattice parameter of magnetite NPs to be (8.399 \AA), which is more close to the standard lattice parameter of magnetite (8.396 \AA).²⁸

To calculate the lattice constant:

$$d = a_0 / \sqrt{h^2 + k^2 + l^2} \quad (1)$$

$$n\lambda = 2d \sin \theta \quad (2)$$

where d is line spacing between planes which can be calculated by Bragg's equation, and a is lattice constant; (hkl) is the indexing plane of atoms which can be obtained from X-ray diffraction data.²⁹

The room temperature hysteresis loops of CoFe_2O_4 and Fe_3O_4 nanoparticles were measured by superconducting

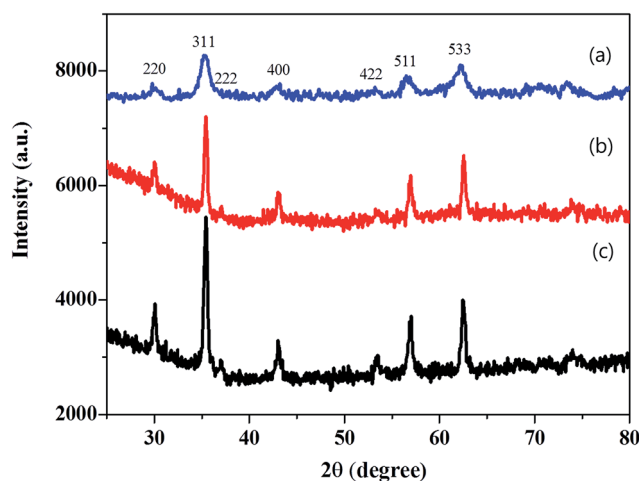


Fig. 6 X-ray diffraction patterns of samples of (a) CoFe_2O_4 nano-sphere, (b) CoFe_2O_4 nanocubes and (c) CoFe_2O_4 nano-hexagonal.

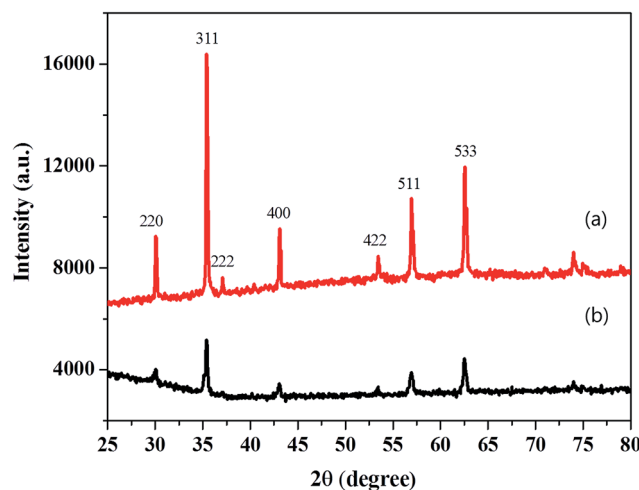


Fig. 7 X-ray diffraction patterns of samples of (a) Fe_3O_4 nanocubes, (b) Fe_3O_4 nano-hexagonal.

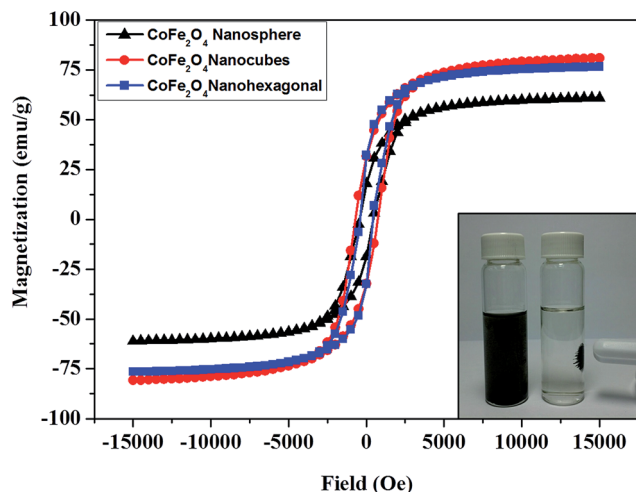


Fig. 8 Hysteresis loops of CoFe_2O_4 nanoparticles measured using SQUID at 300 K and a photograph of CoFe_2O_4 NPs in solution in the absence and presence of an external magnet (inset).

quantum interference device (SQUID) at applied field from -15 kOe to $+15$ kOe. The saturation magnetization value (M_s) of CoFe_2O_4 nanoparticles are 61.1, 80.9 and 76.4 emu per g for the three different shapes of sphere, cube, and hexagonal, respectively (Fig. 8). Hence, it's well known that, the particles with high degree of crystallinity have a surface with negligible spin canting and consequently high magnetic moment value.^{5,30,31} In our samples, the obtained high magnetic moments values for both of cube and hexagonal CoFe_2O_4 nanoparticles is attributed to their high crystallinity structure as clearly appeared and discussed above from the XRD data and TEM images, however, the relatively low magnetization value of 61.1 emu per g for the CoFe_2O_4 NPs sample with sphere shape is may be due to its poor crystallinity and small particle size. The coercivity values (H_c) of the three shapes of sphere, cube and hexagonal CoFe_2O_4 nanoparticles are 439.4, 719.7 and 424.2 Oe, respectively. The difference in the coercivity values with particle size of CoFe_2O_4

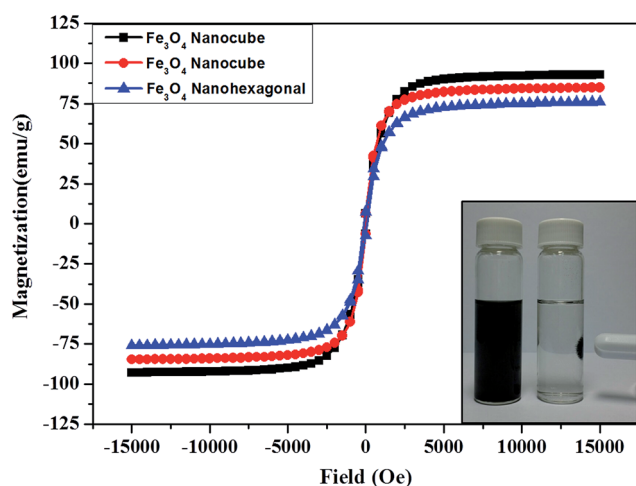


Fig. 9 Hysteresis loops of Fe_3O_4 nanoparticles measured using SQUID at 300 K and a photograph of Fe_3O_4 NPs in solution in the absence and presence of an external magnet (inset).

nanoparticles is may be related to the basis of domain structure, critical size, and the crystalline anisotropy.^{7,32–35}

Fig. 9 shows the magnetization curves for the Fe_3O_4 nanocubes and nanohexagonal. The saturation magnetization value (M_s) of Fe_3O_4 are 92.9, 84.7 and 76 emu per g. The difference in the magnetization values in this case of Fe_3O_4 nanoparticles is also may be due to the difference in the particles size. Apparently, M_s decreases with decreasing particles sizes, and such decrease is ascribed to the surface spin canting and large surface to volume ratio of small nanoparticles.^{36,37} The coercivity value (H_c) of the three samples of Fe_3O_4 are 90.9, 83.3 and 113.6 Oe, respectively. Because of their high magnetic moment values, both of CoFe_2O_4 and Fe_3O_4 nanoparticles can be rapidly separated from solution using an external magnetic field (inset of Fig. 8 and 9).

4. Conclusions

In summary, a facile thermal decomposition approach was successfully designed for the synthesis of highly crystalline CoFe_2O_4 and Fe_3O_4 nanoparticles. Transmission electron microscopy results showed that, three shapes of sphere, cube and hexagonal nanoparticles were obtained through the easy modification of reaction parameters. The CoFe_2O_4 and Fe_3O_4 nanocubes showed the highest magnetic moment values among all of the other nanoparticle shapes. The simple thermal decomposition approach adopted in our work seems to be a very promising route for synthesis of various shapes and sizes of magnetic ferrite materials.

Acknowledgements

This work was supported by the National Research Foundation of Korea (NRF) grant funded by the Korean government (MSIP) (NO.2010-0027963).

References

- 1 D. Ling and T. Hyeon, *Small*, 2013, **9**, 1450–1466.
- 2 J. M. Jeong, B. G. Choi, S. C. Lee, K. G. Lee, S. J. Chang, Y. K. Han, Y. B. Lee, H. U. Lee, S. Kwon, G. Lee, C. S. Lee and Y. S. Huh, *Adv. Mater.*, 2013, **25**, 6250–6255.
- 3 M. B. Gawande, P. S. Branco and R. S. Varma, *Chem. Soc. Rev.*, 2013, **42**, 3371–3393.
- 4 S. C. Goh, C. H. Chia, S. Zakaria, M. Yusoff, C. Y. Haw, S. H. Ahmadi, N. M. Huang and H. N. Lim, *Mater. Chem. Phys.*, 2010, **120**, 31–35.
- 5 M. Abbas, B. P. Rao, M. N. Islam, K. W. Kim, S. M. Naga, M. Takahashi and C. Kim, *Ceram. Int.*, 2014, **40**, 3269–3276.
- 6 F. N. Sayed and V. Polshettiwar, *Sci. Rep.*, 2015, **5**, 09733.
- 7 M. Abbas, B. P. Rao and C. Kim, *Mater. Chem. Phys.*, 2014, **147**, 443–451.
- 8 Y. V. Kolen'ko, M. B. López, C. R. Abreu, E. C. Argibay, A. Sailsman, Y. P. Redondo, M. F. Cerqueira, D. Y. Petrovykh, K. I. Kovnir, O. I. Lebedev and J. Rivas, *J. Phys. Chem. C*, 2014, **118**, 8691–8701.

- 9 Y. Lee, J. Lee, C. J. Bae, J. G. Park, H. J. Noh, J. H. Park and T. Hyeon, *Adv. Funct. Mater.*, 2005, **15**, 3.
- 10 J. Park, K. An, Y. Hwang, J. G. Park, H. J. Noh, J. Y. Kim, J. H. Park, N. M. Hwang and T. Hyeon, *Nat. Mater.*, 2004, **3**, 891–895.
- 11 T. Ahn, J. H. Kim, H. M. Yang, J. W. Lee and J. D. Kim, *J. Phys. Chem. C*, 2012, **116**, 6069–6076.
- 12 M. Abbas, M. Takahashi and C. Kim, *J. Nanopart. Res.*, 2013, **15**, 1354.
- 13 L. T. Lu, N. T. Dung, L. D. Tung, C. T. Thanh, O. K. Quy, N. V. Chuc, S. Maenosonoe and N. T. K. Thanh, *Nanoscale*, 2015, **7**, 19596.
- 14 R. Hufschmid, H. Arami, R. M. Ferguson, M. Gonzales, E. Teeman, L. N. Brush, N. D. Browning and K. M. Krishnan, *Nanoscale*, 2015, **7**, 11142.
- 15 K. Zhang, W. Zuo, Z. Wang, J. Liu, T. Li, B. Wang and Z. Yang, *RSC Adv.*, 2015, **5**, 10632.
- 16 W. Baaziz, B. P. Pichon, Y. Liu, J. M. Grenèche, C. U. Bouillet, E. Terrier, N. Bergeard, V. Halté, C. Boeglin, F. Choueikani, M. Toumi, T. Mhiri and S. B. Colin, *Chem. Mater.*, 2014, **26**, 5063–5073.
- 17 G. Gao, X. Liu, R. Shi, K. Zhou, Y. Shi, R. Ma, E. T. Muromachi and G. Qiu, *J. Am. Chem. Soc.*, 2010, **10**, 2888–2894.
- 18 D. Kim, N. Lee, M. Park, B. H. Kim, K. Jin and T. Hyeon, *J. Am. Chem. Soc.*, 2009, **131**, 454–455.
- 19 H. Yang, T. Ogawa, D. Hasegawa and M. Takahashi, *J. Appl. Phys.*, 2008, **103**, 07D526.
- 20 K. Zhang, W. Zuo, Z. Wang, J. Liu, T. Li, B. Wang and Z. Yang, *RSC Adv.*, 2015, **5**, 10632.
- 21 G. Gao, X. Liu, R. Shi, K. Zhou, Y. Shi, R. Ma, E. T. Muromachi and G. Qiu, *Cryst. Growth Des.*, 2010, **10**, 2888–2894.
- 22 C. Hui, C. Shen, J. Tian, L. Bao, H. Ding, C. Li, Y. Tian, X. Shi and H. J. Gao, *Nanoscale*, 2011, **3**, 701–705.
- 23 M. Abbas, S. R. Torati and C. Kim, *Nanoscale*, 2015, **7**, 12192.
- 24 Y. K. Sun, M. Ma, Y. Zhang and N. Gu, *Colloids Surf., A*, 2004, **245**, 15–19.
- 25 A. L. Andrade, M. A. Valente, J. M. F. Ferreira and J. D. Fabris, *J. Magn. Magn. Mater.*, 2012, **324**, 1753–1757.
- 26 B. D. Cullity, *Elements of X-ray Diffraction*, Addison-Wesley Publication Company Inc, Reading UK, 1956.
- 27 T. J. Shinde, A. B. Gadkari and P. N. Vasambekar, *Mater. Chem. Phys.*, 2008, **111**, 87–91.
- 28 R. M. Cornell and U. Schwertmann, *The Iron Oxides: Structure, Properties, Reactions, Occurrences and Uses*, Wiley-VCH, Weinheim, 2003.
- 29 K. Venkatesan, D. Rajan Babu, M. P. K. Bai, R. Supriya, R. Vidya, S. Madeswaran, P. Anandan, M. Arivanandhan and Y. Hayakawa, *Int. J. Nanomed.*, 2015, **10**, 189–198.
- 30 A. G. Roca, D. Niznansky, V. J. Poltirova, B. Bittova, G. M. A. Fernández, C. J. Serna and M. P. Morale, *J. Appl. Phys.*, 2009, **105**, 1–7.
- 31 M. Abbas, B. P. Rao, S. M. Naga, M. Takahashi and C. Kim, *Ceram. Int.*, 2013, **39**, 7605–7611.
- 32 R. M. Cullity, *Introduction to Magnetic Materials*, Addison-Wesley Publishing, 2nd edn, 1993.
- 33 G. C. Hadjipanayis and R. W. Siegel, *Nanophase Materials Synthesis - Properties - Applications*, Kluwer Academic Publishers, Dordrecht, 1994.
- 34 S. Chikazumi, *Physics of Magnetism*, John Wiley, New York, 1959.
- 35 C. Balasubramanian, Y. B. Kholam, I. Banerjee, P. P. Bakare, S. K. Date, A. K. Das and S. V. Bhoraskar, *Mater. Lett.*, 2004, **58**, 3958–3962.
- 36 Y. Lv, Y. Yang, J. Fang, H. Zhang, E. Peng, X. Liu, W. Xiao and J. Ding, *RSC Adv.*, 2015, **5**, 76764.
- 37 M. P. Morales, S. Veintemillas-Verdaguer, M. I. Montero, C. J. Serna, A. Roig, L. Casas, B. Martínez and F. Sandiumenge, *Chem. Mater.*, 1999, **11**, 3058–3064.